Microchimica Acta (2023) 190:142
https://doi.org/10.1007/s00604-023-05722-1

ORIGINAL PAPER

An electrochemical sensing platform with a molecularly imprinted polymer based on chitosan-stabilized metal@metal-organic frameworks for topotecan detection

Mohammad Mehmandoust[1,2] · Gizem Tiris[3] · Pouran Pourhakkak[4] · Nevin Erk[2] · Mustafa Soylak[5,6,7] · Gulsah S. Kanberoglu[8] · Mehmet Zahmakiran[9]

Received: 13 December 2022 / Accepted: 28 February 2023 / Published online: 18 March 2023

Abstract

The present study aims to develop an electroanalytical method to determine one of the most significant antineoplastic agents, topotecan (TPT), using a novel and selective molecular imprinted polymer (MIP) method for the first time. The MIP was synthesized using the electropolymerization method using TPT as a template molecule and pyrrole (Pyr) as the functional monomer on a metal-organic framework decorated with chitosan-stabilized gold nanoparticles (Au-CH@MOF-5). The materials' morphological and physical characteristics were characterized using various physical techniques. The analytical characteristics of the obtained sensors were examined by cyclic voltammetry (CV), electrochemical impedance spectroscopy (EIS), and differential pulse voltammetry (DPV). After all characterizations and optimizing the experimental conditions, MIP-Au-CH@MOF-5 and NIP-Au-CH@MOF-5 were evaluated on the glassy carbon electrode (GCE). MIP-Au-CH@MOF-5/GCE indicated a wide linear response of 0.4–70.0 nM and a low detection limit (LOD) of 0.298 nM. The developed sensor also showed excellent recovery in human plasma and nasal samples with recoveries of 94.41–106.16 % and 95.1–107.0 %, respectively, confirming its potential for future on-site monitoring of TPT in real samples. This methodology offers a different approach to electroanalytical procedures using MIP methods. Moreover, the high sensitivity and selectivity of the developed sensor were illustrated by the ability to recognize TPT over potentially interfering agents. Hence, it can be speculated that the fabricated MIP-Au-CH@MOF-5/GCE may be utilized in a multitude of areas, including public health and food quality.

Keywords Metal-organic framework application · Molecularly imprinted polymer · Topotecan · Differential pulse voltammetry · Point of care analysis

✉ Mohammad Mehmandoust
mmehmandoust@constructor.university

✉ Nevin Erk
erk@pharmacy.ankara.edu.tr

[1] Department of Life Sciences and Chemistry, Constructor University, 28719 Bremen, Germany

[2] Department of Analytical Chemistry, Faculty of Pharmacy, Ankara University, 06560 Ankara, Turkey

[3] Department of Analytical Chemistry, Faculty of Pharmacy, Bezmialem Vakif University, 34093 Istanbul, Turkey

[4] Department of Chemistry, Payame Noor University (PNU), Tehran, Iran

[5] Department of Chemistry, Faculty of Sciences, Erciyes University, 38039 Kayseri, Turkey

[6] Technology Research & Application Center (TAUM), Erciyes University, 38039 Kayseri, Turkey

[7] Turkish Academy of Sciences (TUBA), Cankaya, Ankara, Turkey

[8] Department of Chemistry, Faculty of Science, Van Yuzuncu Yil University, Van, Turkey

[9] Department of Biotechnology, Faculty of Science, Bartin University, Bartin, Turkey

Introduction

Antineoplastic agents are crucial in treating different types of cancer. Topotecan (TPT), an unoriginal semisynthetic derivative of the plant alkaloid camptothecin, has shown antineoplastic activity in a wide range of cell culture and xenograft systems and is currently recommended for second-line therapy in ovarian and small-cell lung cancer [1]. The significant side effects of TPT usage during chemotherapy are fever, hair loss, sore throat, and chest pain. However, quantifying the chemotherapeutic agent level in the human body is a significant problem for clinical investigations to prevent these adverse effects and analyze the process of cancer therapy [2–4]. Accordingly, various reported strategies have been used for TPT determination, for instance, high liquid chromatography (HPLC) [5] and liquid chromatograph-tandem mass spectrometry (LC-MS/MS) [6].

Notwithstanding some advantages of the reported procedures, most of them often suffer from complexity, expensive equipment, time-consuming, requiring trained personnel, sample manipulations or derivatization steps, and unsatisfied selectivity [7]. Apart from other ways of determination, electrochemical methods offer several different strategies for identifying target analytes with field applicability and basic apparatus [8, 9]. Moreover, the developed electrochemical methods can be manufactured and utilized immediately in biological samples. In that case, it offers a substantial advantage over spectroscopic or chromatographic approaches, which need sample pretreatment and other preparation processes [10–12].

Accordingly, several electrochemical sensors for TPT-sensitive detection based on DNA [13], metal oxide nanoparticles [14], metal nanoparticles [15], ionic liquid [16], and carbon composites [17, 18] have been proposed in the last decade. Nevertheless, many interferences coexisting with TPT in biological samples, including dopamine, uric acid, and ascorbic acid, affect the sensor's detection selectivity and reliability. Besides, many of the previously presented methods employ single-use electrodes, limiting their sensing application for TPT determination in biological samples. As a result, it is crucial to construct effective sensors possessing high selectivity and sensitivity to determine TPT levels for point-of-care (PoC) applications.

The molecularly imprinted polymer (MIP) assay is now a synthetic method for creating particular molecular recognition materials capable of imitating biological receptors, including antibodies and enzymes [19]. After removing template molecules with a suitable solvent, such molecular templating in molecular imprinting polymers leads to the development of selective molecular recognition sites [20]. MIPs outperform natural recognition elements in terms of tunability, inexpensiveness, and simplicity of manufacture. As a result, MIPs are widely used to improve the selectivity of electrochemical sensors [21]. Nevertheless, ordinary MIPs have flaws such as inadequate template removal, poor binding capability, and large diffusion barriers.

Electropolymerization, the most successful approach for producing MIPs, has evolved into a flexible strategy for overcoming the aforementioned issues by deliberately choosing functional monomers and managing the electrochemical parameters [22]. This strategy enables the design of polymers around a template molecule (the analyte) using electropolymerization of monomer. After the polymer is created, the template is washed away, leaving an "imprint" of the analyte template. Ideally, this results in a sorbent capable of highly selective, reversible analyte binding. Bonds form between the polymer and the template during the polymerization process, which may be attributed to the monomeric component's self-assembling [23]. For example, positive charges in the prepolymer will match with negative charges in the template molecule [24]. Nevertheless, this is connected to any noncovalent contact, such as ionic, hydrophobic, π–π, or hydrogen bond interactions. Monomers lead to set interaction areas during polymerization, and even when the template is removed, the resultant cavities duplicate the size and form [25]. These cavities may preferentially incorporate template molecules over structural mimics due to a superior shape and surface chemistry match [26]. The affinity between the template and the monomer should be as strong as possible to enable the imprint molecule's robust binding to the polymer and fixation in the polymer matrix while also allowing for reversibility, indicating that the selected monomer should have complementary functional groups to those found on the template. Accordingly, the electropolymerization of pyrrole (Pyr) has been widely used to fabricate MIP-based electrochemical sensors due to its low cost, semi-conductive behavior, efficient electrochemical properties, and stability [27].

Although MIPs improve selectivity for sensing applications, stochastic imprinting sites are common, resulting in poor recognition efficiency, low adsorption capacity, and slow response [28]. The number of imprinted cavities capable of detecting the target incorporated in the imprinted film greatly influences the sensitivity of MIP-based sensors [29]. To address these concerns, utilizing a supporting material with a wide surface area and high conductivity might allow the imprinted film to be extended and more imprinted sites to be created, boosting sensitivity overall.

Metal-organic frameworks (MOFs) are an intriguing family of structured hybrid porous materials with a high

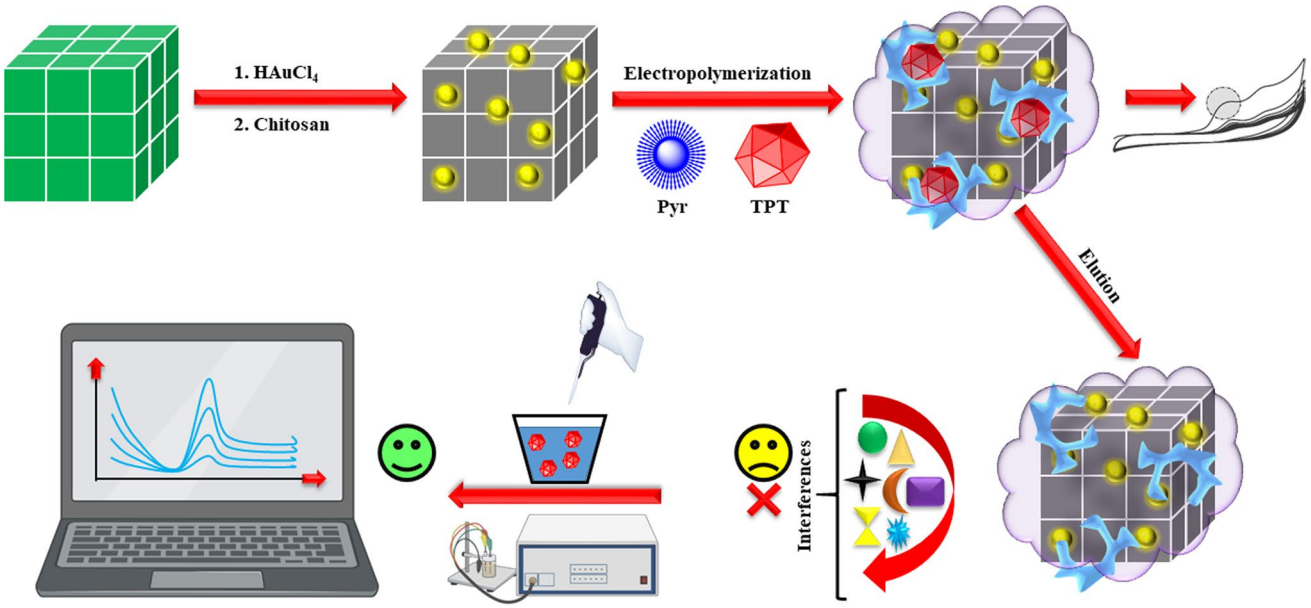

Scheme 1. The procedure for modification of the MIP-Au-CH@MOF-5

cross-sectional area, density, porosity, and dielectric constant [30]. The type of metal utilized in MOFs' structure influences the framework's topology, structure, and pore size [31]. Despite their numerous uses in gas sorption [32], heterogeneous catalysis [33], and energy storage [34], the investigation of MOFs as sensing materials is hampered by their low conductivity and instability in aqueous settings [35]. However, combining MOFs with conductive materials is an excellent technique to increase the electrochemical activity of pristine MOFs, allowing the MOFs to be very adaptable in biomimetic design. Therefore, for this purpose, metal nanoparticles have been utilized as sensor amplifiers to increase the conductivity of MOFs [36, 37].

Recently, gold nanoparticles (Au NPs) have received much interest due to their unique features and technological possibilities. Owing to their remarkable properties, such as optical activity and magnetic properties, as well as their resistance to oxidation and corrosion at high temperatures, Au NPs have been used in many different applications, including medicine [38], fuel [39], and solar cells [40], as well as the manufacture of electrocatalysts and catalysts [41]. There are several methods to synthesize Au NPs with different shapes and activities. For example, recently, Au NPs have been prepared using different reducing agents such as sucrose and borohydride [42]. Moreover, chitosan has lately been employed as a protective agent in the synthesis of Au NPs because it is more than a protecting agent, and gold salt may be reduced to zerovalent gold nanoparticles by chitosan without the use of any additional reducing agent [43]. Chitosan primarily increases the composite's cytocompatibility and biodegradability, whereas Au NPs improve the mechanical, electrical, and catalytic characteristics [44, 45]. As a result, combining chitosan-stabilized Au NPs and MOF-5 with MIPs on the electrode surface might aid in creating innovative sensing devices, significantly improving the performance of electrochemical sensors and opening up new applications.

Here, a novel MIP-based electrochemical sensor was fabricated for in-field monitoring of TPT instead of the traditional analytical platforms. The synergistic effect between the Au NPs, chitosan, and MOF-5 might cause the promising advantages of superior conductivity of the Au NPs, large surface area, and strong adsorption ability of MOF-5. To the best of our knowledge, a novel analytical method was constructed for the TPT analysis based on the MIP strategy for the first time. For this purpose, the Pyr as monomer and TPT as template were electropolymerized onto Au-CH@MOF-5 modified glassy carbon electrode (MIP-Au-CH@MOF-5/GCE, Scheme 1). The experimental variables (number of electropolymerization cycles, template to monomer ratio, elution time, accumulation time, accumulation potential, and pH) were studied and optimized. The as-synthesized MIP-Au-CH@MOF-5/GCE indicated superior sensitivity, selectivity, reproducibility, and stability. In addition, the sensor detected TPT in biological samples with a satisfactory recovery range. It suggests that the developed sensor not only provides a unique PoC analytical method but also increases the utilization of the sensing interface to develop other MIP-based sensors for analytes in biological samples.

Experimental section

The Supplementary Materials contained all the chemicals and equipment used for the experiment and comprehensive experimental instructions.

Results and discussion

Characterization

MOF-5 has been determined to have either a cubic or a tetragonal structure, depending on the synthesis circumstances. However, the cubic structure is more stable than the tetragonal structure [46, 47]. To study the morphology and shape of synthesized MOF-5 and Au-CH@MOF-5 nanostructures, their SEM images are presented in Fig. 1A–D. As shown in Fig. 1A–B, MOF-5 had a smooth surface and a regular hexahedral structure (cube). The particle size distribution was on the order of micrometers, and some of them had angle deficiency. The corresponding SEM images of Au-CH@MOF-5 also showed small Au NPs of primary particles of less than 200.0 nm superimposed at the MOF-5 structures. Meanwhile, as shown in Fig. 1D, no Au NPs agglomeration was found on the surface of the MOF-5, indicating that the porous tunnels of MOF-5 may provide a suitable environment for the growth of Au NPs and restrict them in the tunnel with a small particle size distribution. Moreover, the rigid frameworks might prevent Au NPs from sliding and agglomerating.

The surface roughness of the prepared MOF-5 and Au-CH@MOF-5 was imaged by AFM. As shown in

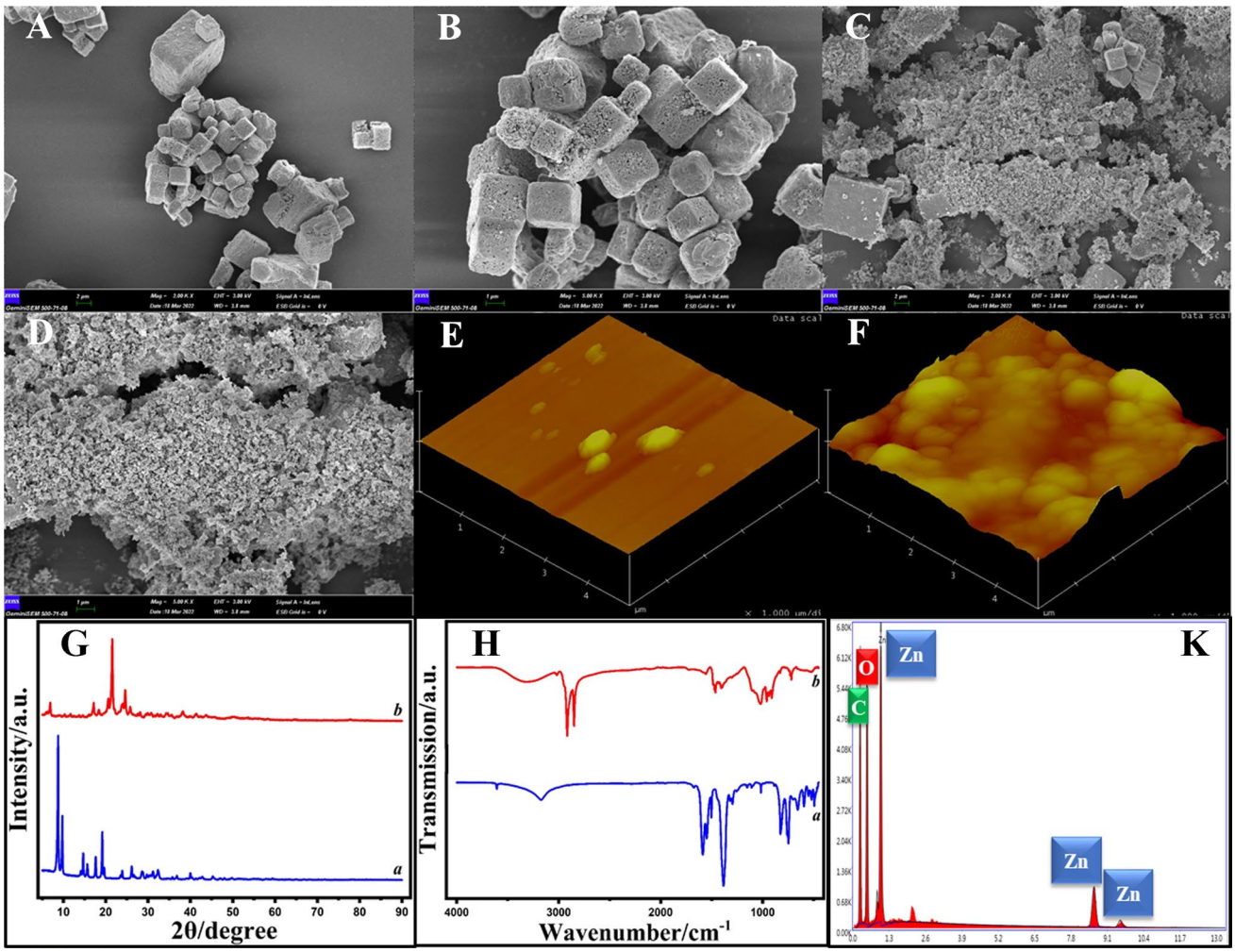

Fig. 1 The SEM image of MOF-5 with different magnifications, 2 μm (**A**) and 1 μm (**B**); Au-CH@MOF-5/GCE with different magnifications, 2 μm (**C**) and 1 μm (**D**); AFM images of MOF-5 (**E**) and Au-CH@MOF-5 (**F**), XRD patterns (**G**), FT-IR spectra (**H**) of MOF-5 (a) and Au-CH@MOF-5 (b), and EDX spectra of MOF-5 (**K**)

Fig. 1F, the Au-CH@MOF-5 exhibited greater roughness and porous features than just MOF-5. The root mean square (RMS) roughness value of the MOF-5 surface was about 7.33 nm, while that of the Au-CH@MOF-5 was 63.0 nm, indicating that more possible imprinted cavities formed on the Au-CH@MOF-5 surface.

Figure 1G demonstrates the XRD patterns of MOF-5 and Au-CH@MOF-5. The characteristic peaks observed at 2θ angle at 9.0°, 9.94°, 14.2°, and 15.5°, which were in good agreement with the reference (PDF card no, 04-0836) [48]. The sharp peak at 9.94° corresponded to the highly crystalline MOF-5. However, the intensity of the peak at 6.9° was diminished in comparison to the peak at 9.94°, demonstrating the anomaly in MOF-5 crystals [49, 50], probably owing to some alteration of atomic orientation in the crystal plane by solvent and other adsorbate molecules that fulfill the mesopores of MOF-5 [51]. By comparing the XRD pattern, the Au-CH@MOF-5 indicated additional diffraction peaks of Au NPs at an upper angle (37.1°, 42.4°), confirming that Au NPs were loaded onto MOF-5. Interestingly, some new reflexes of weak intensity at Au-CH@MOF-5 were observed, which might be ascribed to a crystalline Au phase due to the change in the crystallite sizes in the presence of chitosan. The decrease in intensity of Au-CH@MOF-5 compared to empty MOF-5 gave evidence for pore filling [52].

FT-IR spectrum for the synthesized MOF-5 is illustrated in Fig. 1H. This spectrum is demonstrated in the wavenumber range of 400–4000 cm^{-1}. When the carboxyl group of terephthalic acid was coordinated with the secondary unit ($Zn_4O_6^+$), R-COO- formed an O-C-O resonance structure, thus the peaks at 1600, 1508, and 1388 cm^{-1} corresponded to the C=O symmetric and asymmetric modes [53]. The other bands between 700 to 1700 cm^{-1} also affirmed the presence of benzene ring, including C=C stretching vibration at 1505 cm^{-1} and C-H, O-H bending vibrations at 755, 889, 1019, and 1162 cm^{-1}. Broadband at 3000–3500 cm^{-1} was ascribed to the stretching vibration peak of O-H chemically adsorbed on the MOF surface [54]. In the FT-IR spectra of Au-CH@MOF-5, almost the same absorptions were witnessed with a little shift that indicated the successful modification of Au NPs. However, two more peaks at 2860 and 2930 cm^{-1} were due to C–H vibrations of chitosan, reaffirming the successful synthesis of Au-CH@MOF-5 [55].

Figure 1D displays the EDX spectra of MOF-5 and reveals the existence of C, O, and Zn elements, approving the successful synthesis of MOF-5. Moreover, no extra peak for impurity was observed, indicating high purity and single-phase formation of MOF-5.

Optimization of experimental conditions

The various factors, namely, the number of scan cycles, template to monomer ratio concentration, elution time, accumulation potential, and time, as well as pH, which affect the construction of an efficient MIP-sensor, were examined.

Effect of potential cycle number

The thickness of electropolymerized Pyr is closely related to the scan cycles of CV. The thick Pyr film would partially hinder the charge transfer at the electrode-solution interface; on the other hand, the thicker Pyr might produce more cavities as the recognition site on the MIP surface. As shown in Fig. 2A, with increasing scan cycles from 5.0 to 10.0, the current responses increased up to 10 cycles and then decreased, as well as almost remained unchanged after the 20.0 cycle. Although long cycles promote the development of more imprinted sites, they also produce thicker sensing film with limited site accessibility. As a result, if the generated film is excessively thick, the diffusion of TPT molecules might be negatively affected, with a proportionate effect on the MIP sensor's rebinding capacity and repeatability. Therefore, 10.0 cycles were selected.

Effect of mole ratio

Moreover, to evaluate the effect of the ratio between the monomer and template on the current response of the MIP-Au-CH@MOF-5/GCE, the film was subjected to electropolymerization in solutions of constant TPT concentration and various Pyr concentrations (Fig. 2B). Post the template molecule's removal, the current response of TPT on the developed sensor increased the ratio Pyr to TPT from 1:1 to 1:2. Subsequently, on increasing the ratio, the response remarkably decreased owing to the lesser availability of the number of active binding sites and the non-conducting layer that was formed on increasing the ratio. Therefore, the molar ratio of 1:2 was chosen for the following experiment.

Effect of extraction time

After optimization of the template to monomer ratio concentration and the thickness of the polymeric film, extraction time was studied by immersing the developed electrode in 0.1 M HCl. Template extraction is essential for MIP modification, forming unique recognition sites on the developed electrode surface. The templates should be extracted entirely to avoid influencing the current response. As shown in Fig. 2C, the current response of TPT gradually increased

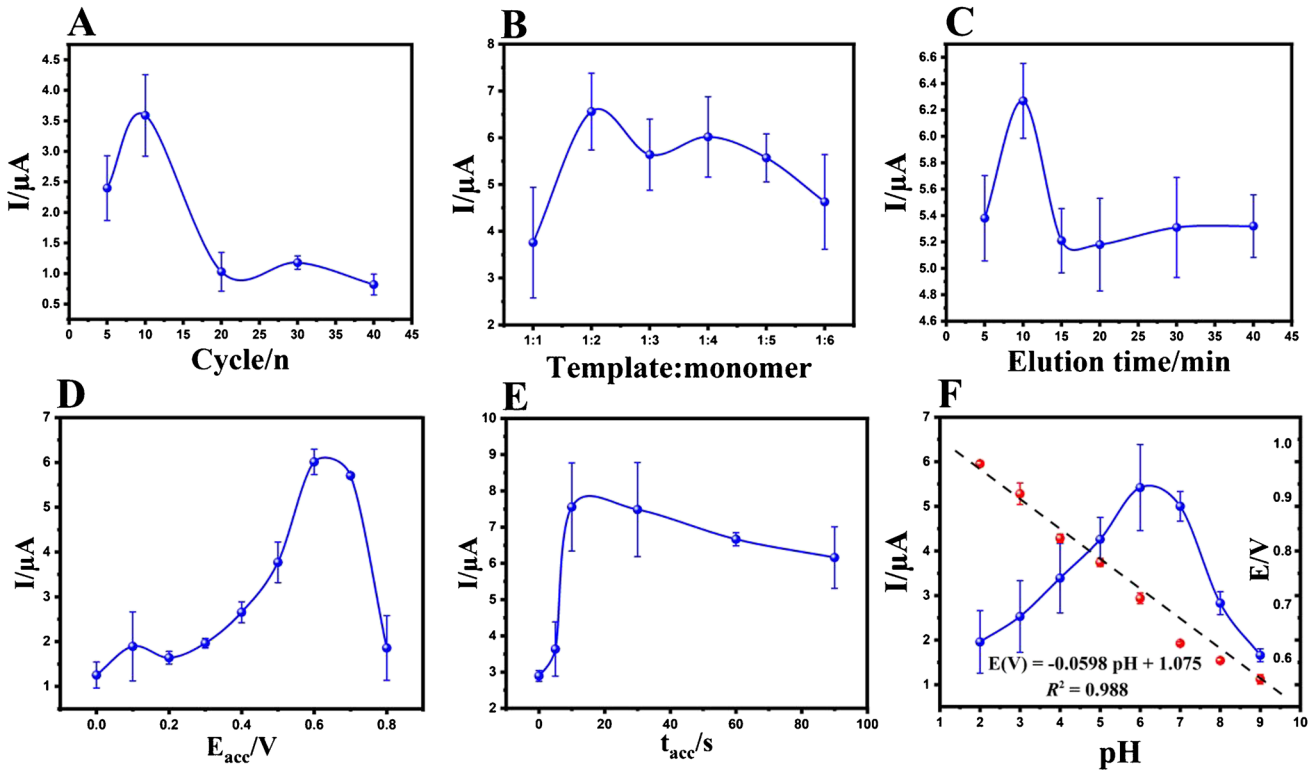

Fig. 2 Effect of the number of the cycle (**A**), template to monomer ratio (**B**), elution time (**C**), accumulation potential (**D**), accumulation time (**E**), and pH in the presence of 0.5 μM TPT in 0.1 M B-R buffer (**F**)

with increasing extraction time from 5.0 to 10.0 min and remained constant from 15.0 to 40.0 min, demonstrating the TPT templates were removed entirely. As a result, the template extraction time was chosen as 10 min in 0.1 M HCl.

Accumulation parameters

The accumulation step is an essential factor in improving the electrochemical sensor's sensitivity in an adsorption-controlled process. The adsorption capability of the MIP-Au-CH@MOF-5/GCE surface was investigated by analyzing the accumulation potential (E_{acc}, Fig. 2D) and time (t_{acc}, Fig. 2E) with DPV in 0.1 M B-R buffer at pH 6.0 containing 0.5 μM TPT. When accumulation potential was varied from +0.8 to 0.0 V at fixed accumulation time (30.0 s), the peak current increased with decreasing accumulation potential from +0.8 to +0.6 V because TPT molecules adsorb better on a more negatively charged surface and gradually leveled off as it changed between 0.6 and 0.0 V due to the instability of the electrode surface during hydrogen evolution. Therefore, the accessible cavities might be more filled by TPT molecules at +0.6 V, consequently increasing electrochemical signals. Hence, a potential of +0.6 V was applied as the accumulation potential.

Moreover, the influence of the accumulation time ranging from 0.0 to 180.0 s on TPT oxidation at MIP-Au-CH@MOF-5/GCE was investigated. The current response reached a stable maximum value with an accumulation time of 10.0 s, after which it was saturated. The phenomenon may be ascribed to the imprinted sites that have been thoroughly combined with target molecules and could not be filled with other molecules anymore after an accumulation period. Therefore, the optimal accumulation time of 10 s was selected for further experiments.

Effect of pH

As an essential parameter to evaluate the developed electrodes, the influence of pH on the electrochemical behavior of 0.5 μM TPT was observed in 0.1 M B-R buffer at various pHs from 2.0 to 9.0 (Fig. 2F). The results showed the highest anodic peak current at pH 6.0, filling more cavities of the MIP template. The current responses of TPT at MIP-Au-CH@MOF-5/GCE remarkably enhanced with the increase of the pH from 2.0 to 6.0 due to the carbonyl group being protonated at a very low pH. Whereas in alkaline conditions (pH>7.0), the current response of TPT decreased when the pH shifted to more alkaline values. However, these

phenomena caused a decrease in TPT binding with MIP, thus lowering the current value. Moreover, the relationship between the oxidation peak potential (Ep) and pH is also shown in Fig. 2F (red dot). A linear shift of E_{pa} toward negative potential upon an increase of pH from 2.0 to 9.0 demonstrated that protons were directly involved in the oxidation of TPT, and it obeyed the following equation: E_{pa} = 1.075–0.0598 pH (R^2=0.988). The slope obtained was close to the theoretical value (0.059 V/pH) and, according to the Nernst equation, suggested the participation of equal numbers of electrons and protons in TPT oxidation, as shown in Scheme S1. The suggested sensor's electro-oxidation mechanism demonstrated that it was an irreversible and sluggish electron transfer process owing to the loss of one electron from the aromatic-OH group due to its oxidation to the carbonyl group.

Effect of scan rate

The kinetic effect of the reaction on the electrode surface was observed with various scan rates from 10.0 to 300.0 mV/s in 0.1 µM TPT using CV, as shown in Fig. S1. The graph indicated an increase in anodic peak with a simultaneous increase in scan rate within a constant potential range from +0.3 to +1.2 V. Accordingly, with the increase of the scan rate, the peak current of TPT increased more linearly with the increase of the scan rate (I=0.0177 v+0.413 (R^2=0.996)) compared to the square root of scan rate (I=0.368 $v^{1/2}$-1.094 (R^2=0.967)), indicating that TPT is an adsorption control process in addition to the diffusion on MIP-Au-CH@MOF-5/GCE. Moreover, peak potentials shifted to an anodic direction with the increase in scan rate, confirming the irreversible character of the electrode reaction. Furthermore, to confirm the electrode reaction process, the influence of logarithm scan rate on the electro-oxidation of TPT was also observed with the following equation: log I (µA) = 0.7 log v+ 1.034 (R^2 = 0.993), reaffirming that the oxidation of TPT at MIP-Au-CH@MOF-5/GCE was mainly controlled by adsorption process in addition to the diffusion.

Characterization of modified electrode

The electrochemical properties of the modified electrodes were recorded by EIS in 5.0 mM $[Fe(CN)_6]^{3-/4-}$ in 0.1 M KCl (Fig. 3A). The BGCE showed a low semicircle with an Rct value of 4.13 kΩ. Nevertheless, after electropolymerization of the polymer, the Rct value increased to 20.96 kΩ for the MIP-Au-CH@MOF-5/GCE and 29.89 kΩ for the NIP-Au-CH@MOF-5/GCE, indicating that the polymeric membrane hindered the charge transfer process. After elution of TPT by immersing in 0.1 M HCl, the Rct of the MIP-Au@MOF-5/GCE was significantly decreased (4.94 kΩ), demonstrating that the imprinted cavities accelerated electron transfer. The rebinding of TPT with the MIP surface was also affirmed by the enhancement in Rct of the MIP-Au-CH@MOF-5/GCE to 14.36 kΩ.

Moreover, a step-by-step characterization of GCE modifications was performed through CV using a solution of 5.0 mM $[Fe(CN)_6]^{3-/4-}$ in 0.1 M KCl. As shown in Fig. 3B, two well-defined redox peaks were observed using a bare electrode. However, the redox peaks' magnitude after electropolymerization of Pyr on the Au-CH@MOF-5 surface in the absence of TPT (NIP-Au-CH@MOF-5/GCE) was reduced, which could be related to the non-conductive coating polymer, preventing electrolyte ions from reaching the electrode surface. Moreover, the redox signal of MIP-Au-CH@MOF-5/GCE after elution was higher than that of MIP-Au-CH@MOF-5/GCE before elution and NIP-electrodes in two states before and after elution due to created 3D-holes after elution facilitates diffusion of ions to the surface, leading to generating high electrical signals. Interestingly, when the MIP-Au-CH@MOF-5/GCE was incubated in 20.0 µM TPT solution for 60 s, the electrochemical response of the sensor was remarkably decreased, demonstrating that the polymer

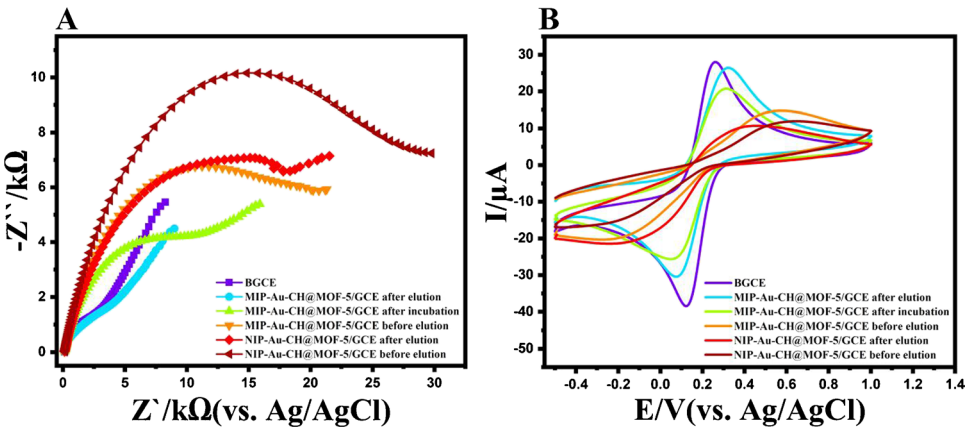

Fig. 3 EISs (**A**) and CVs (**B**) of BGCE, MIP-Au-CH@MOF-5/GCE after elution, MIP-Au-CH@MOF-5/GCE after incubation, MIP-Au-CH@MOF-5/GCE before elution, NIP-Au-CH@MOF-5/GCE after elution, NIP-Au-CH@MOF-5/GCE before elution in the presence of 5.0 mM $[Fe(CN)_6]^{3-/4-}$ in 0.1 M KCl at scan rate of 50.0 mV S^{-1}

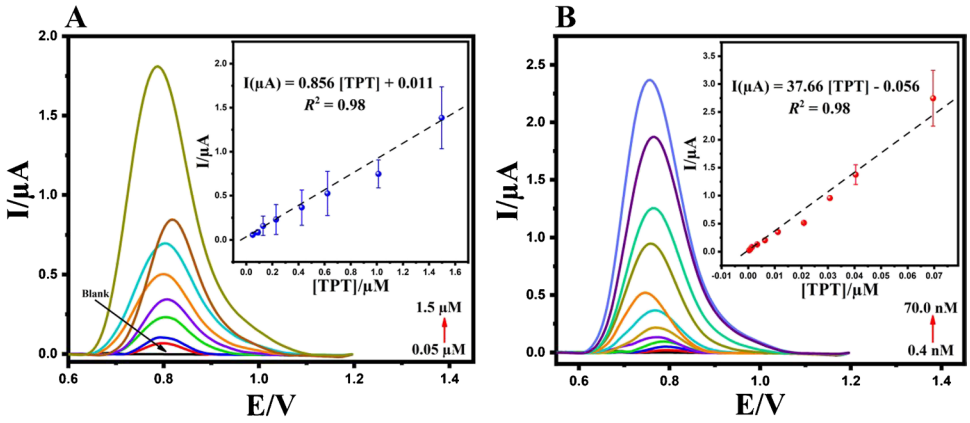

Fig. 4 DPVs at NIP-Au-CH@MOF-5/GCE in various concentrations of TPT from 0.05 to 1.5 μM (**A**) and MIP-Au-CH@MOF-5/GCE in various concentrations of TPT from 0.4 to 70.0 nM (**B**). (Stripping conditions: accumulation potential of 0.6 V and accumulation time of 10 s). Error bars represent the standard deviation for at least three independent measurements

sites being occupied by TPT and redox probe molecules could not easily hit the electrode surface. These phenomena in the response of the MIP-Au-CH@MOF-5/GCE after ousting the template and after incubation in the template solution indicated that TPT molecules were introduced into the Pyr film during the electropolymerization, approving that the imprinted sensor was successfully prepared.

Analytical application

The DPV responses and the calibration curve for the electrochemical determination of TPT using the MIP-Au-CH@MOF-5/GCE under optimal experimental conditions were investigated. As shown in Fig. 4A, sharp DPV peaks were observed for low TPT levels. Afterward, TPT's wide linear concentration range was evaluated by increasing TPT concentration in 0.1 M B-R buffer (pH 6.0) at MIP-Au-CH@MOF-5/GCE. The oxidation current of TPT enhanced linearly as the TPT concentration increased from 0.4 up to 70.0 nM. Fig. 4A (inset) indicates the calibration plot of TPT. The linear regression equation was I(μA)=37.66 [TPT]-0.056 (R^2=0.98) with a low LOD of 0.2987 nM (3SD/m) [56]. The improved detection ability of Au-CH@MOF-5 was due to the electrocatalytic properties of Au NPs and MOF-5, as well as favorable electrostatic interactions and π-stacking interactions. Furthermore, the Pyr linkers have a high π-electron density, which is predicted to interact strongly with the π-electrons of the TPT phenyl moieties, providing a stable channel for electron transfer.

No TPT-specific binding sites were predicted to identify the target TPT at the NIP-Au-CH@MOF-5/GCE. On the other hand, the low current responses resulted from TPT non-specific adsorption on the NIP surface. Consequently, the DPV responses were obviously lower than that at the MIP-Au-CH@MOF-5/GCE, and the linear regression equation was expressed as I(μA)=0.856 [TPT]-0.011 (R^2=0.98).

The imprinting factor (IF) is one of the selectivity criteria for MIP-based sensors, and its value is related to the sensor's effectiveness in identifying the target analyte [57, 58]. The IF was estimated based on the sensitivity ratio at the MIP-Au-CH@MOF-5/GCE to the NIP-Au-CH@MOF-5/GCE [59]. The calculated imprinting factor is equal to 44.0, suggesting the superior binding ability of the MIP.

To assess the detection effect of MIP-Au-CH@MOF-5/GCE on TPT, the different approaches for TPT determination are summarized in Table 1. The developed electrode showed an excellent linear relationship and an ultralow LOD of 0.298 nM. In addition, the most important benefit of this

Table 1 Comparison of the MIP-Au-CH@MOF-5/GCE with other electrodes for the detection of TPT

Method	Modifier	Linear range (μM)*	LOD (μM)*	Real sample	Ref.
SWV	nano-AB-Au NPs	0.00199–0.671	0.0000164	Blood serum-urine	[15]
SWV	NrG/MOICl	0.6–800	0.27	Injection-pharmaceutical serum	[16]
SWV	1-BPr/CuO	0.7–800	0.3	Injection	[14]
DPV	Au NRDs/MI-GR	0.1–16.0	0.022	Blood serum	[60]
DPV	ds-DNA graphene	0.7-90.0	0.37	Blood serum-urine	[61]
DPV	2D-MoS_2/TiO_2	0.01–18.57	0.0098	Plasma-urine	[62]
SWV	TiO_2/GRP/CHIT	0.21–2.62	0.26	Tablet	[17]
DPV	AB film	4.36–873.5	3.16	Blood serum	[63]
DPV	MIP-Au-CH@MOF-5	0.0004–0.07	0.000298	Saliva-plasma	This work

*The units have been standardized

proposed technique is that it can swiftly extract the pattern and assess TPT by applying a potential of 0.6 V and a short duration of 10.0 s, while the molded film has a selective absorption of species. Another advantage of this method is the ability to use the developed sensor in actual samples without affecting other drugs, eliminating interference from real samples with complex matrices.

However, all comparison electrodes studied have their own advantages or disadvantages in terms of synthesis and fabrication. For instance, nano-AB-AuNPs/GCPE showed a LOD as low as 0.0161 nM. Although the electrode is easy to use, its application is hampered by its cost and inflexibility for fabrication as a disposable electrode. Besides, most previous reports were applied to analyze the samples containing low matrices and did not study the tolerance for interferences in saliva samples. These literature comparisons emphasized that our MIP-Au-CH@MOF-5/GCE suggests an acceptable LOD and wide concentration range for TPT detection than previously reported sensors. This pointed out that our sensor has a superior potential application for monitoring the safety of on-site analysis.

Selectivity

To investigate the selectivity of the MIP-Au-CH@MOF-5/GCE, the influences of some possible interfering agents, including ascorbic acid, dopamine, uric acid, L-arginine, L-cysteine, glucose, K^+, NO_3^-, Cl^-, Na^+, PO_4^{3-}, OH^-, and Ba^{2+} on peak currents and potentials of TPT, were examined by the DPV technique (Fig. S2). It was found that 200-fold excess of interferences did not interfere with detecting TPT, demonstrating that the developed sensor had a superior anti-interference capability. The complementarity of the binding site on the electrode surface with the structure of the TPT in the imprinting cavity, as well as the stiff structure of the MIP, contributed to this capacity.

Repeatability, reproducibility, and stability

The repeatability, reproducibility, and stability are crucial for evaluating electrochemical sensors' practicability and applicability. The repeatability of Au-CH@MOF-5/GCE was investigated in 0.01 μM TPT for ten consecutive tests with a single sensor, and their currents and potentials were almost entirely coincident with a relative standard deviation (RSD) less than 6.0%, indicating that MIP-Au-CH@MOF-5/GCE possessed superior repeatability (Fig. S3). Moreover, the reproducibility was evaluated from the DPV current response to TPT at three different MIP-Au-CH@MOF-5/GCE independently under the same condition. The RSD of reproducibility of the developed electrode was estimated at 5.7%, suggesting the superior reproducibility of MIP-Au-CH@MOF-5/GCE (Fig. S4). Furthermore, MIP-Au-CH@MOF-5/GCE was stored at room temperature and followed for 3 weeks to investigate its long-term stability. The current response maintained around 94.5 % of the initial measured value after 3 weeks, exhibiting the remarkable stability of MIP-Au-CH@MOF-5/GCE (Fig. S5).

Table 2 Determination of TPT in saliva and human plasma samples

Sample	Added (nM)	Found	RSD (%)	Recovery (%)
Saliva	3.0	3.04	0.13	101.37
	10.0	9.5	0.06	95.07
	50.0	53.52	2.33	107.05
Human plasma	3.0	2.83	0.032	94.41
	10.0	9.52	0.053	95.25
	50.0	53.08	3.89	106.16

Real sample analysis

To evaluate the benefits of the developed sensor in a real-world application, the analysis of TPT was performed in real samples, including human plasma and saliva. The analysis was carried out using the established technique after spiking the real samples with varying concentrations of TPT. As indicated in Table 2, the recoveries of the real sample ranged from 94.4 to 107.3%, with an RSD of less than 4.0 %, confirming the suitability of the established concept for TPT analysis in real samples.

Conclusion

This work addresses the development of a new approach to the direct electrochemical detection of TPT based on MIP integrated with Au-CH@MOF-5 nanocomposite. The Au-CH@MOF-5 improved the sensitivity with a large surface area and low electron transfer resistance. The developed electrode showed a low LOD of 0.298 nM and wide linear concentration range of 0.4 to 70.0 nM. Moreover, the creation of the MIP that acted as an artificial recognizer membrane increased the selectivity of the TPT determination. The as-synthesized polymer on Au-CH@MOF-5/GCE allowed numerous benefits over normal electrode sensors for TPT determination. The promising electrostatic attraction between the positively charged TPT and the negatively charged modified polymer enabled better analyte contact with the electrode surface and accelerated the electron transfer. It is considered that MIP-Au-CH@MOF-5/GCE showed a development evaluation suitable for use in actual analytical applications, such as clinical

and biomedical applications in the PoC technology devices sector. The forthcoming analytes detection electrode sensors of platforms or system enhancements that should be costless, sensitive, and take less time to detect analyte levels would be very near to being available everywhere.

Supplementary information The online version contains supplementary material available at https://doi.org/10.1007/s00604-023-05722-1.

Funding This work was supported by the Scientific Research Projects Commission of Ankara University (Project Number: 21B0237005). Dr. M. Soylak is grateful for the financial support of the unit of the scientific research projects of Erciyes University (FYL-2021-11170) (Kayseri, Turkey).

Declarations

Conflict of interest The authors declare no competing interests.

References

1. Ormrod D, Spencer CM (1999) Topotecan. A review of its efficacy in small cell lung cancer. Drugs 58:533–551. https://doi.org/10.2165/00003495-199958030-00020/METRICS
2. Karimi-Maleh H, Shojaei AF, Tabatabaeian K et al (2016) Simultaneous determination of 6-mercaptopruine, 6-thioguanine and dasatinib as three important anticancer drugs using nanostructure voltammetric sensor employing Pt/MWCNTs and 1-butyl-3-methylimidazolium hexafluoro phosphate. Biosens Bioelectron 86:879–884. https://doi.org/10.1016/J.BIOS.2016.07.086
3. Alavi-Tabari SAR, Khalilzadeh MA, Karimi-Maleh H (2018) Simultaneous determination of doxorubicin and dasatinib as two breast anticancer drugs uses an amplified sensor with ionic liquid and ZnO nanoparticle. J Electroanal Chem 811:84–88. https://doi.org/10.1016/J.JELECHEM.2018.01.034
4. Karimi-Maleh H, Karimi F, Alizadeh M, Sanati AL (2020) Electrochemical sensors, a bright future in the fabrication of portable kits in analytical systems. Chem Rec 20:682–692. https://doi.org/10.1002/TCR.201900092
5. Rosing H, Doyle E, Davies BE, Beijnen JH (1995) High-performance liquid chromatographic determination of the novel antitumour drug topotecan and topotecan as the total of the lactone plus carboxylate forms, in human plasma. J Chromatogr B Biomed Sci Appl 668:107–115. https://doi.org/10.1016/0378-4347(95)00054-M
6. Ye L, Shi J, Wan S et al (2013) Development and validation of a liquid chromatography–tandem mass spectrometry method for topotecan determination in beagle dog plasma and its application in a bioequivalence study. Biomed Chromatogr 27:1532–1539. https://doi.org/10.1002/BMC.2956
7. Mehmandoust M, Pourhakkak P, Hasannia F et al (2022) A reusable and sensitive electrochemical sensor for determination of Allura red in the presence of Tartrazine based on functionalized nanodiamond@SiO2@TiO2; an electrochemical and molecular docking investigation. Food Chem Toxicol 164:113080. https://doi.org/10.1016/J.FCT.2022.113080
8. Tiris G, Khoshnavaz Y, Öven EN et al (2022) A sensitive voltammetric sensor for specific recognition of vitamin C in human plasma based on MAPbI3 perovskite nanorods: Original scientific paper. J Electrochem Sci Eng 12:175–183. https://doi.org/10.5599/JESE.1153
9. Mehmandoust M, Karimi F, Erk N (2022) A zinc oxide nanorods/molybdenum disulfide nanosheets hybrid as a sensitive and reusable electrochemical sensor for determination of anti-retroviral agent indinavir. Chemosphere 300:134430. https://doi.org/10.1016/J.CHEMOSPHERE.2022.134430
10. Altunay N, Elik A, Tuzen M et al (2023) Determination and extraction of acrylamide in processed food samples using alkanol-based supramolecular solvent-assisted dispersive liquid-liquid microextraction coupled with spectrophotometer: optimization using factorial design. J Food Compos Anal 115:105023. https://doi.org/10.1016/J.JFCA.2022.105023
11. Mohebbi A, Jouyban A, Farajzadeh MA et al (2022) Combination of mixed mode dispersive solid phase extraction with magnetic ionic liquids based dispersive liquid–liquid microextraction for the extraction of anticoagulant drugs from urine samples. Microchem J 183:108065. https://doi.org/10.1016/J.MICROC.2022.108065
12. MarziKhosrowshahi E, AfsharMogaddam MR, Javadzadeh Y et al (2022) Experimental and density functional theoretical modeling of triazole pesticides extraction by Ti2C nanosheets as a sorbent in dispersive solid phase extraction method before HPLC-MS/MS analysis. Microchem J 178:107331. https://doi.org/10.1016/J.MICROC.2022.107331
13. Congur G, Erdem A, Mese F (2015) Electrochemical investigation of the interaction between topotecan and DNA at disposable graphite electrodes. Bioelectrochemistry 102:21–28. https://doi.org/10.1016/J.BIOELECHEM.2014.11.003
14. Alavi-Tabari SAR, Khalilzadeh MA, Karimi-Maleh H, Zareyee D (2018) An amplified platform nanostructure sensor for the analysis of epirubicin in the presence of topotecan as two important chemotherapy drugs for breast cancer therapy. New J Chem 42:3828–3832. https://doi.org/10.1039/C7NJ04430E
15. Ibrahim M, Ibrahim H, Almandil NB, Kawde AN (2018) A novel nanocomposite based on gold nanoparticles loaded on acetylene black for electrochemical sensing of the anticancer drug topotecan in the presence of high concentration of uric acid. J Electroanal Chem 824:22–31. https://doi.org/10.1016/J.JELECHEM.2018.07.031
16. Mohammadian A, Ebrahimi M, Karimi-Maleh H (2018) Synergic effect of 2D nitrogen doped reduced graphene nano-sheet and ionic liquid as a new approach for fabrication of anticancer drug sensor in analysis of doxorubicin and topotecan. J Mol Liq 265:727–732. https://doi.org/10.1016/J.MOLLIQ.2018.07.026
17. Saxena S, Shrivastava R, Satsangee SP, Srivastava S (2014) TiO 2 /graphene/chitosan-nanocomposite-based electrochemical sensor for the sensing of anti-HIV drug topotecan. J Electrochem Soc 161:H934–H940. https://doi.org/10.1149/2.0891414JES/XML
18. Bavandpour R, Rajabi M, Asghari A (2022) Electrochemical determination of epirubicin in the presence of topotecan as essential anti-cancer compounds using paste electrode amplified with Pt/SWCNT nanocomposite and a deep eutectic solvent. Chemosphere 289:133060. https://doi.org/10.1016/J.CHEMOSPHERE.2021.133060
19. Erk N, Mehmandoust M, Soylak M (2022) Electrochemical sensing of favipiravir with an innovative water-dispersible molecularly imprinted polymer based on the bimetallic metal-organic framework: comparison of morphological effects. Biosensors 12:769. https://doi.org/10.3390/BIOS12090769/S1
20. Martín-Esteban A (2001) Molecularly imprinted polymers: new molecular recognition materials for selective solid-phase extraction of organic compounds. Anal Bioanal Chem 370:795–802. https://doi.org/10.1007/S002160100854/METRICS
21. Mehmandoust M, Erk N, Naser M, Soylak M (2023) Molecularly imprinted polymer film loaded on the metal–organic framework with improved performance using stabilized gold-doped graphite carbon nitride nanosheets for the single-step detection of Fenamiphos. Food Chem 404:134627. https://doi.org/10.1016/J.FOODCHEM.2022.134627
22. Rahman S, Bozal-Palabiyik B, Unal DN et al (2022) Molecularly imprinted polymers (MIPs) combined with nanomaterials as

electrochemical sensing applications for environmental pollutants. Trends Environ Anal Chem 36:e00176. https://doi.org/10.1016/J.TEAC.2022.E00176
23. Wackerlig J, Schirhagl R (2016) Applications of molecularly imprinted polymer nanoparticles and their advances toward industrial use: a review. Anal Chem 88:250–261. https://doi.org/10.1021/ACS.ANALCHEM.5B03804/ASSET/IMAGES/LARGE/AC-2015-038045_0005.JPEG
24. Arabi M, Ostovan A, Li J et al (2021) Molecular imprinting: green perspectives and strategies. Adv Mater 33:2100543. https://doi.org/10.1002/ADMA.202100543
25. Zhang N, Zhang N, Xu Y et al (2019) Molecularly imprinted materials for selective biological recognition. Macromol Rapid Commun 40:1900096. https://doi.org/10.1002/MARC.201900096
26. Hart BR, Rush DJ, Shea KJ (2000) Discrimination between enantiomers of structurally related molecules: separation of benzodiazepines by molecularly imprinted polymers. J Am Chem Soc 122:460–465. https://doi.org/10.1021/JA9926313/ASSET/IMAGES/LARGE/JA9926313H00002.JPEG
27. Jin H, Guo H, Gao X, Gui R (2018) Selective and sensitive electrochemical sensing of gastrodin based on nickel foam modified with reduced graphene oxide/silver nanoparticles complex-encapsulated molecularly imprinted polymers. Sensors Actuators B Chem 277:14–21. https://doi.org/10.1016/J.SNB.2018.08.156
28. Ding S, Lyu Z, Niu X et al (2020) Integrating ionic liquids with molecular imprinting technology for biorecognition and biosensing: a review. Biosens Bioelectron 149:111830. https://doi.org/10.1016/J.BIOS.2019.111830
29. Yang B, Fu C, Li J, Xu G (2018) Frontiers in highly sensitive molecularly imprinted electrochemical sensors: challenges and strategies. TrAC Trends Anal Chem 105:52–67. https://doi.org/10.1016/J.TRAC.2018.04.011
30. Abdelhamid HN, Sharmoukh W (2021) Intrinsic catalase-mimicking MOFzyme for sensitive detection of hydrogen peroxide and ferric ions. Microchem J 163:105873. https://doi.org/10.1016/J.MICROC.2020.105873
31. Abdelhamid HN, Georgouvelas D, Edlund U, Mathew AP (2022) CelloZIFPaper: cellulose-ZIF hybrid paper for heavy metal removal and electrochemical sensing. Chem Eng J 446:136614. https://doi.org/10.1016/J.CEJ.2022.136614
32. Zhao Y, Wang J, Bao Z et al (2018) Adsorption separation of acetylene and ethylene in a highly thermostable microporous metal-organic framework. Sep Purif Technol 195:238–243. https://doi.org/10.1016/J.SEPPUR.2017.11.044
33. Schlichte K, Kratzke T, Kaskel S (2004) Improved synthesis, thermal stability and catalytic properties of the metal-organic framework compound Cu3(BTC)2. Microporous Mesoporous Mater 73:81–88. https://doi.org/10.1016/J.MICROMESO.2003.12.027
34. Wang L, Han Y, Feng X et al (2016) Metal–organic frameworks for energy storage: Batteries and supercapacitors. Coord Chem Rev 307:361–381. https://doi.org/10.1016/J.CCR.2015.09.002
35. Mehmandoust M, Erk EE, Soylak M et al (2022) Metal–organic framework based electrochemical immunosensor for label-free detection of glial fibrillary acidic protein as a biomarker. Ind Eng Chem Res. https://doi.org/10.1021/ACS.IECR.2C01445
36. Wang H, Chen W, Chen Q et al (2021) Metal-organic framework (MOF)-Au@Pt nanoflowers composite material for electrochemical sensing of H2O2 in living cells. J Electroanal Chem 897:115603. https://doi.org/10.1016/J.JELECHEM.2021.115603
37. Dong J, Zhang D, Li C et al (2022) A sensitive electrochemical sensor based on PtNPs@Cu-MOF signal probe and DNA walker signal amplification for Pb2+ detection. Bioelectrochemistry 146:108134. https://doi.org/10.1016/J.BIOELECHEM.2022.108134
38. Mahapatra I, Sun TY, Clark JRA et al (2015) Probabilistic modelling of prospective environmental concentrations of gold nanoparticles from medical applications as a basis for risk assessment. J Nanobiotechnology 13:1–14. https://doi.org/10.1186/S12951-015-0150-0/FIGURES/3
39. Wang X, Falk M, Ortiz R et al (2012) Mediatorless sugar/oxygen enzymatic fuel cells based on gold nanoparticle-modified electrodes. Biosens Bioelectron 31:219–225. https://doi.org/10.1016/J.BIOS.2011.10.020
40. Notarianni M, Vernon K, Chou A et al (2014) Plasmonic effect of gold nanoparticles in organic solar cells. Sol Energy 106:23–37. https://doi.org/10.1016/J.SOLENER.2013.09.026
41. Xue ZH, Zhang SN, Lin YX et al (2019) Electrochemical reduction of N2 into NH3 by donor-acceptor couples of Ni and Au nanoparticles with a 67.8% faradaic efficiency. J Am Chem Soc 141:14976–14980. https://doi.org/10.1021/JACS.9B07963/ASSET/IMAGES/LARGE/JA9B07963_0004.JPEG
42. da Silva AB, Rufato KB, de Oliveira AC et al (2020) Composite materials based on chitosan/gold nanoparticles: from synthesis to biomedical applications. Int J Biol Macromol 161:977–998. https://doi.org/10.1016/J.IJBIOMAC.2020.06.113
43. Huang H, Yang X (2004) Synthesis of chitosan-stabilized gold nanoparticles in the absence/presence of tripolyphosphate. Biomacromolecules 5:2340–2346. https://doi.org/10.1021/BM0497116/SUPPL_FILE/BM0497116SI20040514_034954.PDF
44. Komenek S, Luesakul U, Ekgasit S et al (2017) Nanogold-gallate chitosan-targeted pulmonary delivery for treatment of lung cancer. AAPS PharmSciTech 18:1104–1115. https://doi.org/10.1208/S12249-016-0644-6/FIGURES/8
45. Dhahri A, Serghei A, Farzi G et al (2016) Chitosan-dithiooxamide-grafted rGO sheets decorated with Au nanoparticles: synthesis, characterization and properties. Eur Polym J 78:153–162. https://doi.org/10.1016/J.EURPOLYMJ.2016.03.023
46. Huang L, Wang H, Chen J et al (2003) Synthesis, morphology control, and properties of porous metal–organic coordination polymers. Microporous Mesoporous Mater 58:105–114. https://doi.org/10.1016/S1387-1811(02)00609-1
47. Kaye SS, Dailly A, Yaghi OM, Long JR (2007) Impact of preparation and handling on the hydrogen storage properties of Zn4O(1,4-benzenedicarboxylate)3 (MOF-5). J Am Chem Soc 129:14176–14177. https://doi.org/10.1021/JA076877G/SUPPL_FILE/JA076877GSI20071011_065658.PDF
48. Nivetha R, Gothandapani K, Raghavan V et al (2021) Nano-MOF-5 (Zn) derived porous carbon as support electrocatalyst for hydrogen evolution reaction. ChemCatChem 13:4342–4349. https://doi.org/10.1002/CCTC.202100958
49. Saha D, Deng S, Yang Z (2009) Hydrogen adsorption on metal-organic framework (MOF-5) synthesized by DMF approach. J Porous Mater 16:141–149. https://doi.org/10.1007/S10934-007-9178-3/TABLES/4
50. Tsukamoto Y, Mabuchi K, Barbara Panella B, Hirscher M (2005) Hydrogen physisorption in metal–organic porous crystals. Adv Mater 17:538–541. https://doi.org/10.1002/ADMA.200400946
51. Hafizovic J, Bjørgen M, Olsbye U et al (2007) The inconsistency in adsorption properties and powder XRD data of MOF-5 is rationalized by framework interpenetration and the presence of organic and inorganic species in the nanocavities. J Am Chem Soc 129:3612–3620. https://doi.org/10.1021/JA0675447/SUPPL_FILE/JA0675447SI20070105_040009.PDF
52. Esken D, Zhang X, Lebedev OI et al (2009) Pd@MOF-5: limitations of gas-phase infiltration and solution impregnation of [Zn4O(bdc)3] (MOF-5) with metal–organic palladium precursors for loading with Pd nanoparticles. J Mater Chem 19:1314–1319. https://doi.org/10.1039/B815977G
53. Askari H, Ghaedi M, Dashtian K, Azghandi MHA (2017) Rapid and high-capacity ultrasonic assisted adsorption of ternary toxic anionic dyes onto MOF-5-activated carbon: Artificial neural networks, partial least squares, desirability function and isotherm

and kinetic study. Ultrason Sonochem 37:71–82. https://doi.org/10.1016/J.ULTSONCH.2016.10.029
54. Sun X, Li Y (2004) Colloidal carbon spheres and their core/shell structures with noble-metal nanoparticles. Angew Chemie Int Ed 43:597–601. https://doi.org/10.1002/ANIE.200352386
55. Srivastava M, Srivastava SK, Nirala NR, Prakash R (2014) A chitosan-based polyaniline–Au nanocomposite biosensor for determination of cholesterol. Anal Methods 6:817–824. https://doi.org/10.1039/C3AY41812J
56. Mehmandoust M, Mehmandoust A, Erk N (2022) Construction of a simple and selective electrochemical sensor based on Nafion/TiO2 for the voltammetric determination of olopatadine: Original scientific paper. J Electrochem Sci Eng 12:91–103. https://doi.org/10.5599/JESE.1117
57. Nantasenamat C, Naenna T, Isarankura Na-Ayudhya C, Prachayasittikul V (2005) Quantitative prediction of imprinting factor of molecularly imprinted polymers by artificial neural network. J Comput Aided Mol Des 19:509–524. https://doi.org/10.1007/S10822-005-9004-4/METRICS
58. Mehdinia A, Aziz-Zanjani MO, Ahmadifar M, Jabbari A (2013) Design and synthesis of molecularly imprinted polypyrrole based on nanoreactor SBA-15 for recognition of ascorbic acid. Biosens Bioelectron 39:88–93. https://doi.org/10.1016/J.BIOS.2012.06.052
59. Ayerdurai V, Cieplak M, Noworyta KR et al (2021) Electrochemical sensor for selective tyramine determination, amplified by a molecularly imprinted polymer film. Bioelectrochemistry 138:107695. https://doi.org/10.1016/J.BIOELECHEM.2020.107695
60. Er E, Erk N (2020) A novel electrochemical sensing platform based on mono-dispersed gold nanorods modified graphene for the sensitive determination of topotecan. Sensors Actuators B Chem 320:128320. https://doi.org/10.1016/J.SNB.2020.128320
61. Beitollahi H, Dehghannoudeh G, Moghaddam HM, Forootanfar H (2017) A sensitive electrochemical DNA biosensor for anticancer drug topotecan based on graphene carbon paste electrode. J Electrochem Soc 164:H812–H817. https://doi.org/10.1149/2.0511712JES/XML
62. Mehmandoust M, Çakar S, Özacar M et al (2021) (2021) Electrochemical sensor for facile and highly selective determination of antineoplastic agent in real samples using glassy carbon electrode modified by 2D-MoS2 NFs/TiO2 NPs. Top Catal 1:1–13. https://doi.org/10.1007/S11244-021-01479-0
63. Cheng Q, Du Y, Wu K et al (2011) Electrochemical detection of anticancer drug topotecan using nano-acetylene black film. Colloids Surf B Biointerfaces 84:135–139. https://doi.org/10.1016/J.COLSURFB.2010.12.027